Vibrational energy relaxation in classical fluids. II. High-frequency spectra in liquids

Max Teubner[a] and Dirk Schwarzer[b]
Max-Planck-Institut für biophysikalische Chemie, Postfach 2841, 37077 Göttingen, Germany

(Received 13 March 2003; accepted 30 April 2003)

A procedure is outlined to determine high-frequency spectra of classical liquids interacting via Lennard-Jones and similar potentials and applied to the problem of vibrational energy relaxation. The theory is based on analytical expressions derived for spherical particles in gases [Paper I, D. Schwarzer and M. Teubner, J. Chem. Phys. **116**, 5680 (2002)] and is extended to the dense liquid phase by considering binary collisions in the potential of mean force. The calculated spectra are in good agreement with those derived from classical trajectory and molecular dynamics simulations. © *2003 American Institute of Physics.* [DOI: 10.1063/1.1585018]

I. INTRODUCTION

Vibrational energy relaxation (VER) of excited molecules plays a key role in chemical dynamics because very often the outcome of a chemical reaction is determined by the competition between reactive steps and vibrational energy transfer. Therefore, over the last decades great experimental and theoretical efforts have been expended to ascertain the main factors affecting VER processes in the gas and the liquid phase.[1–9]

The simplest energy relaxation mechanism involves the transfer of vibrational energy into translational degrees of freedom of the bath. The theoretical description of this process is usually based on first-order perturbation theory. One finds that the classical VER rate of a harmonic oscillator with frequency ω_0 in a thermal environment is given by[10–14]

$$k_{\mathrm{ver}}=\frac{1}{2\mu k_{\mathrm{B}}T}S_F(\omega_0), \tag{1}$$

where μ is the reduced mass of the oscillator and k_{B} and T are the Boltzmann constant and the temperature, respectively. $S_F(\omega)$ is the power spectrum of the fluctuating solvent force $F(t)$ exerted on the solute vibrational coordinate while its bond is held rigid,

$$S_F(\omega)=\int_{-\infty}^{\infty}\cos(\omega t)\langle F(t)F(0)\rangle dt. \tag{2}$$

In principle, the force–force time-correlation function appearing in Eq. (2) should be evaluated at a quantum level.[15] Reliable and tractable methods to derive this quantity, however, are not available for interacting many-body systems. Thus, just the classical correlation function is usually used and certain corrections factors are introduced to account for quantum effects.[16–19]

A widely used method to derive the classical spectrum is to calculate $S_F(\omega)$ directly from an equilibrium molecular dynamics simulation. However, in the case of high-frequency oscillators this is a challenging problem for several reasons.[20] First, the dynamic range of the Fourier transform of the force–force time-correlation function is usually limited by the numerical accuracy to 16 orders of magnitude, such that the high-frequency spectral range often is not accessible. Second, spectra at high frequency are determined by rare high-energy collisions. To properly sample these collisions, the simulation time can become prohibitively large. And, finally, computer simulations are usually done in finite ensembles with fixed total energy underestimating the probability of high-energy collisions with respect to a Boltzmann distribution. Accordingly, the calculated spectral density at high frequency is lower than expected from a canonical ensemble, even for an infinitely long simulation time.

Therefore, a theory to calculate $S_F(\omega)$ at high frequencies, at least for simple cases, is desirable. Employing the breathing sphere model we have developed such a theory for the gas phase[20] (Paper I), i.e., at conditions where only binary interactions between colliders have to be considered. For particles interacting via Lennard-Jones and similar potentials expressions for the spectra were derived which are asymptotically exact and of the form $S_F(\omega)\propto\exp[-(\omega\tau)^\nu]$, where exponent ν and time constant τ depend only on the interaction potential. Since the exponent was shown to be $\nu\leqslant 2/3$, the spectra decay always slower than exponentially in contrast to the popular exponential energy gap law.[21–23] The result, however, is in agreement with the more qualitative theory of Landau and Teller[24] which, for the special case of a repulsive exponential potential, found $\nu=2/3$.

In this paper we will extend our theory to derive high-frequency spectra for liquids. As in Paper I the theory is applied to the vibrational energy relaxation of a breathing sphere in an atomic environment. Our approach takes advantage of the fact that at high frequencies all collective motion of the solvent is frozen. The only processes which contribute to the spectra in this frequency domain are rare high-energy binary collisions as in the gas phase. This is the basis of the independent binary collision (IBC) model.[1,6,25–28] Within this approach the complicated many-body dynamics reduces to the two-body problem of binary collisions in a static poten-

[a]Electronic mail: mteubne@gwdg.de
[b]Electronic mail: dschwar@gwdg.de

tial. In the gas-phase the trajectory associated with a collision is determined simply by the binary potential between the molecules. In the liquid the static potential of the frozen environment has to be added. In principle, the static potential of the environment changes between collisions. In our theory, however, we take the average and approximate it by the potential of mean force. With respect to the binary interactions the potential of mean force is treated as a small perturbation.

The paper is organized as follows: In the next section we briefly summarize the analytical results of Paper I[20] and Ref. 29 obtained for spectra of spherical particles in dilute gases. In Sec. III the theory is extended to the liquid phase and approximate expressions for corresponding high-frequency spectra are derived. We apply the theory to the problem of vibrational energy relaxation by introducing the breathing sphere model in Sec. IV. In Sec. V a Monte Carlo method is presented to sample $g(r)$ at short distances relevant for high-energy collisions. Finally, the theory is compared with trajectory and molecular dynamics simulations.

II. SPECTRA IN DILUTE GASES

In this section we briefly review the general theory[20,29] which studies the high-frequency spectra of binary observables in dilute classical gases.

Consider a dilute gas of density ρ. A relative binary observable $A=A(t)$ associated with a tagged particle i is a sum of local observables,

$$A=\sum_{j\neq i} A_{\mathrm{loc}}, \tag{3}$$

where each $A_{\mathrm{loc}}=A_{\mathrm{loc}}(t)$ depends only on the relative trajectory $\mathbf{r}_{ij}=\mathbf{r}_i-\mathbf{r}_j$ of a pair of particles at time t. We also require that A_{loc} tends to zero for large separation. Examples for functions A_{loc} are the potential $V(r_{ij}(t))$ or the force $-V'(r_{ij}(t))$ between the particles. We are interested in the spectrum

$$S_A(\omega)=\int_{-\infty}^{\infty} dt\; e^{i\omega t}(\langle A(t)A(0)\rangle-\langle A\rangle^2). \tag{4}$$

In a dilute gas of density ρ and in the high-frequency range the spectrum can be written in the form

$$S_A(\omega)=\int_0^{\infty} dE\int_0^{\infty} dl\; Z(E,l)|A_{\mathrm{loc}}(\omega)|^2, \tag{5}$$

where

$$Z(E,l)=4\pi\rho(2\pi\mu k_{\mathrm{B}}T)^{-3/2}e^{-\beta E}2\pi l \tag{6}$$

is the number density of collisions with energy E and angular momentum l per unit time. Here $\mu=m/2$ is the reduced mass, $\beta=(k_{\mathrm{B}}T)^{-1}$, and

$$A_{\mathrm{loc}}(\omega)=\int_{-\infty}^{\infty} dt\; e^{i\omega t}A_{\mathrm{loc}}(t) \tag{7}$$

is the Fourier transform of $A_{\mathrm{loc}}(t)=A_{\mathrm{loc}}(r(t))$.

In the following we often take as local observable A_{loc} an inverse power of the distance of the colliding pair

$$r^{-p}(\omega)=\int_{-\infty}^{\infty} dt\,\frac{e^{i\omega t}}{r(t)^p}, \tag{8}$$

and assume that the potential $V(r)$ is analytic in the whole complex r-plane with the exception of a singularity at the origin where the dominant term is

$$V(r)\sim\frac{A}{r^n},\quad r\sim 0. \tag{9}$$

Under these conditions the spectrum can be asymptotically evaluated in the high-frequency range with the result

$$S_A(\omega)\sim a(\omega\tau)^{\sigma}e^{-\mathrm{Min}_E(\beta E+2\omega t^*(E))}, \tag{10}$$

where a is an amplitude, τ is a time constant, and t^* is defined by

$$t^*(E)=\sqrt{\frac{\mu}{2}}\int_0^{r_0}\frac{dr}{\sqrt{V(r)-E}}. \tag{11}$$

r_0 is the turning point given by $V(r_0)=E$ [for sufficiently high energy any potential of the form Eq. (9) has a single turning point]. t^* depends on the details of the potential, but τ depends only on the dominant singularity Ar^{-n}, while a and σ depend in addition on p. Exponent σ is given by

$$\sigma=\frac{4p}{n+2}-\frac{5n+8}{3n+2}. \tag{12}$$

Since A has dimension energy$\times$length^n, it is convenient to replace A by a length r_{th} defined by

$$A=k_{\mathrm{B}}Tr_{\mathrm{th}}^n. \tag{13}$$

Then time constant τ and amplitude a are given by

$$\tau=c_0 r_{\mathrm{th}}\sqrt{2\mu\beta}, \tag{14}$$

$$a=\alpha(\rho r_{\mathrm{th}}^3)\tau r_{\mathrm{th}}^{-p}. \tag{15}$$

The numerical constants c_0 and α are

$$c_0=\sqrt{\pi}(1-\nu)^{-1/\nu}\frac{\Gamma\left(\frac{1}{\nu}\right)}{\Gamma\left(\frac{1}{n}\right)} \tag{16}$$

and

$$\alpha=4\pi c_0\left(\frac{2\pi}{\Gamma(p\lambda)}\right)^2((n+2)c_0)^{-2p\lambda}\frac{n}{\nu}\times\sqrt{2\nu(1-\nu)}(1-\nu)^{1-2/n}\frac{\Gamma\left(\frac{1}{2}+\frac{1}{n}\right)\Gamma\left(1-\frac{1}{n}\right)}{\Gamma\left(\frac{3}{2}-\frac{1}{n}\right)\Gamma\left(\frac{1}{n}\right)}, \tag{17}$$

with

$$\nu=\frac{2n}{3n+2}. \tag{18}$$

For special potentials more explicit results can be obtained. In the simplest situation the potential has the form Eq. (9) everywhere. Then

$$t^*(E)=\tau\frac{\nu}{2}\left(\frac{1-\nu}{\beta E}\right)^{(1/\nu)-1}, \tag{19}$$

the minimum can be performed, and Eq. (10) becomes

$$S_A(\omega)\sim a(\omega\tau)^{\sigma}e^{-(\omega\tau)^{\nu}}. \tag{20}$$

The main contribution to the spectra comes from energies near

$$\beta E(\omega)=(1-\nu)(\omega\tau)^{\nu}. \tag{21}$$

For the Lennard-Jones potential,

$$V_{\mathrm{LJ}}(r)=4\epsilon\left(\left(\frac{\sigma}{r}\right)^{12}-\left(\frac{\sigma}{r}\right)^{6}\right), \tag{22}$$

Eq. (10) becomes in the high-frequency limit,

$$S_{\mathrm{LJ}}(\omega)\sim a(\omega\tau)^{\sigma}e^{-(\omega\tau)^{12/19}+0.408\,88\sqrt{\kappa}(\omega\tau)^{6/19}+0.126\,511\kappa}, \tag{23}$$

where $\kappa=4\epsilon/k_{\mathrm{B}}T$ and $n=12$ in Eqs. (12)–(18). For high frequency the main contribution to the spectra comes from energies near

$$\beta E(\omega)\sim\tfrac{7}{19}(\omega\tau)^{12/19}-0.279\,76\sqrt{\kappa}(\omega\tau)^{6/19}-0.126\,511\kappa. \tag{24}$$

This is similar to Shin[30] but differs in the frequency-independent terms.

III. SPECTRA IN LIQUIDS

A. General remarks

We now turn to our main subject, high-frequency spectra in dense fluids.

At very low-frequency, spectra in fluids are simple and have universal features. They are determined by the collective motion of many particles and can be described by macroscopic hydrodynamics involving a few phenomenological constants.[31] In the intermediate range, where the inverse frequency is comparable to the collision time, the problem seems complicated because hydrodynamics becomes unreliable while multibody correlations must still be taken into account. At high frequency, however, the situation drastically simplifies again.

(1) As in gases, at high frequency the spectra are dominated by rare binary collisions with high energy.
(2) The high-frequency spectra are dominated by a small region near the turning point where the particle spends only a very short time. During this time the configuration of the environment is practically unchanged. Therefore we again have scattering in a time-independent potential.
(3) Davis and Oppenheim[26] have argued that high-energy collisions are not independent but occur in groups. While this is true, it has been shown previously[29] that the collisions dominating the high-frequency spectra are almost central. In fact, the higher the frequency, the less noncentral collisions contribute to the spectra.[29] Consider now an almost central collision. Even if the colliding particles retain most of their energy, the probability that one of the particles makes a second central collision is overwhelmingly small. It it this stringent condition on centrality, that guarantees that the collisions seen in the high-frequency spectra are independent, even in a dense liquid.

We conclude that the high-frequency spectra in fluids, as in gases, are determined by independent binary collisions in a static potential. The situation differs form a gas only insofar as the potential is different in every collision.

The potential is a sum of the direct pair potential $V(r)$ and a perturbation $\delta V(\mathbf{r})$ which is due to the environment. In general, the perturbing potential $\delta V(\mathbf{r})$ is noncentral, but it is analytic and bounded near $r=0$ (it is, however, singular at the positions of the neighbors). At any given moment, the environment essentially has three different effects on a colliding pair: A force accelerates the pair, a torque rotates it, and a compression or dilation along the radius vector $\mathbf{r}$ acts like a radial potential. The first two effects are small and we expect them to be completely negligible at high frequencies. Furthermore, they do not affect observables like r^{-p} that depend only on the distance. The third effect, however, does modify the spectra somewhat and is equivalent to a spherically symmetric perturbation $\delta V(r)$. Using Eq. (10), this suggests that the spectra in a dense liquid in the high-frequency domain can be written in the form

$$S_A(\omega)\sim a(\omega\tau)^{\sigma}\langle e^{-\mathrm{Min}_E(\beta E+2\omega t^*_{V+\delta V}(E))}\rangle, \tag{25}$$

where the average is over the different δV generated by the environment and

$$t^*_{V+\delta V}(E)=\sqrt{\frac{\mu}{2}}\int_0^{r_0}\frac{dr}{\sqrt{V(r)+\delta V(r)-E}}. \tag{26}$$

Now it is important to note that $\delta V(r)$ is bounded and analytic at $r=0$. Since a, τ, and σ depend only on the asymptotic features of the potential near $r=0$, these quantities have the same values as in the gas phase. Therefore, the ratio of the spectra in the liquid and the gas phase is given by

$$\frac{\rho_{\mathrm{gas}}}{\rho_{\mathrm{liq}}}\frac{S_{\mathrm{liq}}(\omega)}{S_{\mathrm{gas}}(\omega)}\sim\frac{\langle e^{-\mathrm{Min}_E(\beta E+2\omega t^*_{V+\delta V}(E))}\rangle}{e^{-\mathrm{Min}_E(\beta E+2\omega t^*_{V}(E))}}. \tag{27}$$

The right hand side can be evaluate using Monte Carlo or molecular dynamics with moderate effort. We prefer, however, to proceed in a semianalytic way which better illuminates the physical issues involved and permits us to introduce some approximations.

B. Approximations

In the spirit of mean field theory we assume that the fluctuations of the potential δV in different environments are of minor importance, and that it is sufficient to study scattering in some effective or average potential. We will argue below that a good candidate for this potential is the potential of mean force $V_{\mathrm{mf}}(r)=-k_{\mathrm{B}}T\ln g(r)$.

Let us write

$$\delta\overline{V}(r)=\delta V(r)-\delta V(r_0), \tag{28}$$

where r_0 is the turning point. Replace $\delta V(r)$ by $\delta V(r_0) + \delta\overline{V}(r)$ in $t^*_{V+\delta V}$. Then

$$t^*_{V+\delta V}(E) = t^*_{V+\delta\overline{V}}(E - \delta V(r_0)), \tag{29}$$

and we may write Eq. (27) in the form

$$\frac{\rho_{\rm gas}}{\rho_{\rm liq}} \frac{S_{\rm liq}(\omega)}{S_{\rm gas}(\omega)} \sim \left\langle e^{-\beta\delta V(r_0)} \frac{e^{-{\rm Min}_E(\beta E + 2\omega t^*_{V+\delta\overline{V}}(E))}}{e^{-{\rm Min}_E(\beta E + 2\omega t^*_V(E))}} \right\rangle. \tag{30}$$

It has been stated below that the high-frequency spectra are determined by the potential in the vicinity of the turning point. Since $\delta\overline{V}(r_0) = 0$, the potentials V and $V + \delta\overline{V}$ have the same values at the turning point. Their effect only differs by the force $-\delta\overline{V}'$ from the environment which is very small compared to the direct force at close separation.

1. IBC and improved IBC approximation

As our first approximation, let us neglect the force from the environment altogether. Then we obtain

$$\frac{\rho_{\rm gas}}{\rho_{\rm liq}} \frac{S_{\rm liq}(\omega)}{S_{\rm gas}(\omega)} \sim \langle e^{-\beta\delta V(r_0)} \rangle. \tag{31}$$

In order to relate δV to known quantities note that in this approximation the particles experience precisely the same force during their collision in the liquid as in the gas. This implies that the ratio of the spectra depends on static quantities only and

$$\frac{S_{\rm liq}(\omega)}{S_{\rm gas}(\omega)} = \frac{N_{\rm liq}(r_0)}{N_{\rm gas}(r_0)}, \tag{32}$$

where $N(r_0)$ is the number density of pairs with a turning point at r_0. The right-hand side is equal to the ratio of the equilibrium pair distribution functions,

$$\frac{\rho_{\rm gas}}{\rho_{\rm liq}} \frac{S_{\rm liq}(\omega)}{S_{\rm gas}(\omega)} = \frac{g_{\rm liq}(r_0)}{g_{\rm gas}(r_0)}, \tag{33}$$

or

$$\frac{\rho_{\rm gas}}{\rho_{\rm liq}} \frac{S_{\rm liq}(\omega)}{S_{\rm gas}(\omega)} = e^{-\beta(V_{\rm mf}(r_0) - V(r))}, \tag{34}$$

where $V_{\rm mf}$ is the potential of mean force. Comparing, we find that in this approximation the effective potential in a fluid is the potential of mean force.

Equation (33) is essentially the IBC approximation of Oppenheim and Davis.[26] However, while it is not obvious from the previous work what values should be taken for the turning point, this follows easily from our results.

Indeed, r_0 is defined by $V(r_0) + \delta V(r_0) = E_{\rm liq}(\omega)$, where $E_{\rm liq}(\omega)$ is the energy minimizing $\beta E + 2\omega t^*_{V+\delta V}(E)$. According to Eq. (29), $t^*_{V+\delta V}(E) = t^*_V(E - \delta V(r_0))$ where we have neglected $\delta\overline{V}$ in the spirit of the IBC approximation. This implies

$$E_{\rm liq}(\omega) = E_{\rm gas}(\omega) + \delta V(r_0), \tag{35}$$

and therefore the turning point can be obtained from

$$V(r_0) = E_{\rm gas}(\omega). \tag{36}$$

The dominant energies $E_{\rm gas}(\omega)$ in the gas phase for the potential Ar^{-n} and the Lennard-Jones potential are given by Eqs. (21) and (24), respectively. Approximation (33) in conjunction with (36) is our improved IBC approximation which we test below.

2. Mean field theory

The IBC approximation rests on the assumption that the only effect of the environment is a redefinition of the energy level by the potential of the mean force at the turning point. Now we try to improve upon this approximation. We retain the assumption that the relevant potential for the high-energy collisions is the potential of mean force, but we no longer neglect the force from the environment.

As a first step we must estimate $t^*_{V+\delta\overline{V}}(E)$ for large E. Since $\delta\overline{V}(r)$ is finite while $V(r)$ diverges for $r \to 0$, we have for small r,

$$\frac{\delta\overline{V}(r)}{V(r) - V(r_0)} \ll 1, \tag{37}$$

and may expand as

$$\begin{aligned} t^*_{V+\delta\overline{V}}(E) &= \sqrt{\frac{\mu}{2}} \int_0^{r_0} \frac{1}{(V(r) - V(r_0) + \delta\overline{V}(r))^{1/2}} dr \\ &\sim \sqrt{\frac{\mu}{2}} \int_0^{r_0} \frac{1}{(V(r) - V(r_0))^{1/2}} \\ &\quad \times \left(1 - \frac{1}{2} \frac{\delta\overline{V}(r)}{V(r) - V(r_0)} \right) dr + \cdots \\ &= t^*_V(E) - \frac{1}{2} \sqrt{\frac{\mu}{2}} \int_0^{r_0} \frac{\delta\overline{V}(r)}{(V(r) - V(r_0))^{3/2}} dr \\ &\quad + \cdots. \end{aligned} \tag{38}$$

For potentials satisfying Eq. (9) it is easy to see that the neglected terms are of order $t^*_V(E)(\beta E)^{-2}$. With

$$\begin{aligned} \lambda(r_0) = \frac{1}{2} &\left(\int_0^1 \frac{ds}{\left(\frac{V(r_0 s)}{V(r_0)} - 1 \right)^{1/2}} \right)^{-1} \\ &\times \int_0^1 \frac{\beta\delta V(r_0 s) - \beta\delta V(r_0)}{\left(\frac{V(r_0 s)}{V(r_0)} - 1 \right)^{3/2}} ds, \end{aligned} \tag{39}$$

we write Eq. (38) in the form

$$\frac{t^*_{V+\delta\overline{V}}(E)}{t^*_V(E)} = 1 - \frac{\lambda(r_0)}{\beta E} + O((\beta E)^{-2}). \tag{40}$$

$\lambda(r_0)$ is of order 1 for potentials satisfying Eq. (9).

The next step is to minimize $\beta E + 2\omega t^*_{V+\delta\overline{V}}(E)$ with respect to E. To first order (i.e., for sufficiently large βE) this minimum is given by the value at $E_V = E_V(\omega)$ which minimizes $\beta E + 2\omega t^*_V(E)$. Denoting ${\rm Min}\{\beta E + 2\omega t^*_{V+\delta\overline{V}}(E)\}$ by ${\rm Min}_{V+\delta\overline{V}}$, etc. we find in the high-energy region,

$$\mathrm{Min}_{V+\delta V}=\beta E_V+2\omega t_V^*(E_V)-2\omega t_V^*(E_V)\frac{\lambda(r_0)}{\beta E_V}$$

$$=\mathrm{Min}_V-(\mathrm{Min}_V-\beta E_V)\frac{\lambda(r_0)}{\beta E_V}. \tag{41}$$

Comparing with Eqs. (20) and (21) we find, that in the high-frequency region,

$$\frac{\mathrm{Min}_V}{\beta E_V}\sim\frac{1}{1-\nu}, \tag{42}$$

and therefore we obtain finally

$$\frac{\rho_{\mathrm{gas}}}{\rho_{\mathrm{liq}}}\frac{S_{\mathrm{liq}}(\omega)}{S_{\mathrm{gas}}(\omega)}\sim e^{-\beta\delta V(r_0)+\eta(r_0)}, \tag{43}$$

where

$$\eta(r_0)=\frac{\nu}{1-\nu}\lambda(r_0). \tag{44}$$

This differs from the Davis–Oppenheim result by the factor $e^{\eta(r_0)}$.

If $V(r)$ varies much stronger near the turning point than $\delta V(r)$, we can approximate

$$\eta(r_0)\sim\frac{\nu}{2(1-\nu)}r_0\beta\delta V'(r_0)\left(\int_0^1\frac{ds}{\left(\frac{V(r_0s)}{V(r_0)}-1\right)^{1/2}}\right)^{-1}$$

$$\times\int_0^1\frac{s-1}{\left(\frac{V(r_0s)}{V(r_0)}-1\right)^{3/2}}ds. \tag{45}$$

For the homogeneous potential Ar^{-n} the integrals can be evaluated with the result

$$\eta(r_0)\sim r_0\beta\delta V'(r_0)\left(1-\frac{1}{2}\frac{\Gamma\left(\frac{1}{n}\right)\Gamma\left(\frac{3}{2}+\frac{2}{n}\right)}{\Gamma\left(\frac{2}{n}\right)\Gamma\left(\frac{3}{2}+\frac{1}{n}\right)}\right). \tag{46}$$

In particular for $n=12$,

$$\eta(r_0)\sim-0.045\,69r_0\beta\delta V'(r_0). \tag{47}$$

IV. VIBRATIONAL ENERGY RELAXATION OF A BREATHING SPHERE

In order to calculate vibrational energy relaxation rates and corresponding spectral densities $S_F(\omega)$ by means of our theory, the oscillator and its vibrational coordinate have to be spherically symmetric. Such a ''breathing sphere'' model has been used in numerous studies to predict the density dependence of VER rates of diatomic[22] or even more complex molecules.[32] According to Egorov and Skinner,[22] the diameter of the breathing sphere is $\sigma_{\mathrm{BS}}=\sigma_0+q$, where q describes deviations from the equilibrium value σ_0. When the breathing sphere collides with a bath particle of diameter σ_s the interaction is determined by the effective diameter $(\sigma_s+\sigma_0+q)/2$. The perturbing force acting on the vibrational coordinate is given by

$$F=\sum_i f(r_i)=-\sum_i\left.\frac{\partial V(r_i,q)}{\partial q}\right|_{q=0}, \tag{48}$$

where $f(r)$ is the binary force and the summation is over all the bath particles. Considering the repulsive V_{12} and the Lennard-Jones potential,

$$V_{12}(r)=\varepsilon\left(\frac{\sigma}{r}\right)^{12}, \tag{49}$$

$$V_{\mathrm{LJ}}(r)=4\varepsilon\left[\left(\frac{\sigma}{r}\right)^{12}-\left(\frac{\sigma}{r}\right)^{6}\right], \tag{50}$$

the binary forces are

$$f_{12}(r)=-6\frac{\varepsilon}{\sigma}\left(\frac{\sigma}{r}\right)^{12} \tag{51}$$

and

$$f_{\mathrm{LJ}}(r)=-12\frac{\epsilon}{\sigma}\left[2\left(\frac{\sigma}{r}\right)^{12}-\left(\frac{\sigma}{r}\right)^{6}\right], \tag{52}$$

respectively.

The effective interaction parameters are given by $\sigma=(\sigma_s+\sigma_0)/2$ and $\varepsilon=\sqrt{\varepsilon_s\varepsilon_0}$, where ε_s and ε_0 are the well depths of solvent and solute, respectively.

Note that for the repulsive potential the binary breathing sphere force is proportional to the potential energy. In the case of the Lennard-Jones potential the same is true for the leading repulsive terms which dominate the high-frequency spectrum. Therefore, the potential energy spectra of Eqs. (20) and (23) have to be multiplied by $(6/\sigma)^2$ to get the corresponding force spectra. A comparison of Eqs. (49) and (50) with (9) and (13) implies $r_{\mathrm{th}}=\sigma^{12}\sqrt{\varepsilon/(k_{\mathrm{B}}T)}$ for the repulsive potential, whereas for the Lennard-Jones potential $r_{\mathrm{th}}=\sigma^{12}\sqrt{4\varepsilon/(k_{\mathrm{B}}T)}$ holds.

For our simulations we simplify the model by considering the special case of a neat liquid corresponding to $\sigma=\sigma_s=\sigma_0$, $\varepsilon=\varepsilon_s=\varepsilon_0$, and $m=m_s=m_0=2\mu$. This procedure improves the statistics of the molecular dynamics simulations considerably, because each particle can be treated as a solute. To present our data we use reduced spatial and time units: $\overline{r}=r/\sigma$ and $\overline{t}=t\sqrt{\varepsilon/2\mu\sigma^2}$. Accordingly, dimensionless forces and force power spectra are defined as $\overline{F}=F\sigma/\varepsilon$ and $\overline{S_F}=S_F\sigma\sqrt{1/2\mu\varepsilon^3}$. Reduced temperature and density are $\overline{T}=k_{\mathrm{B}}T/\varepsilon$ and $\overline{\rho}=\rho\sigma^3$, respectively.

V. SIMULATION METHODS

The theory is compared with two types of numerical methods, namely classical molecular dynamics simulations in an NVE ensemble and classical trajectory simulations of single collisions in a potential of mean force. For all calculations the temperature was $\overline{T}=1.0$.

A. Molecular dynamics simulations

Molecular dynamics (MD) simulations were performed in a cubic simulation box with periodic boundary conditions containing 108–1372 particles. The density was adjusted to

$\bar{\rho}=0.85-0.90$. Equations of motions were integrated with a time step of $\Delta\bar{t}=0.001$ applying the leap-frog algorithm. "Shifted-force potentials" of the form[23,33]

$$V^{\mathrm{SF}}(r)=\left[V(r)-V(R_c)-\left(\frac{dV(r)}{dr}\right)_{r=R_c}(r-R_c)\right]\theta(R_c-r), \tag{53}$$

were used to prevent high-frequency artefacts in the spectra [$\theta(x)$ is the Heaviside step function]. This method keeps forces (in particular, breathing sphere forces) continues at the cutoff distance R_c by adding a small linear term to the potential. For all simulations R_c was set equal to half the box length.

After equilibration the breathing sphere force $F_i(t)$ acting on each particle i was recorded for up to 2^{24} time steps. The power spectrum was calculated by first dividing the time series into overlapping segments of 2^{14} steps length (neighboring segments overlap over 3/4 of their length), multiplying each segment with a Hanning window function,[34] performing the Fourier transform by applying the Wiener–Khintchine theorem, and averaging over all the segments and particles. These numerical calculations were performed with double precision.

B. Classical trajectory simulations

In order to numerically demonstrate the validity of the mean field approximation for high-frequency spectra, the phase space integral Eq. (5) is calculated by repetitively simulating binary collisions of two particles moving in the relevant potential of mean force. The impact parameter is varied between $b=0$ and a maximum $b_{\max}$ beyond which interactions between colliders are negligible. The initial kinetic energy is varied between 0 and $E_{\max}$ with $E_{\max}$ being in the range $(40-50)k_{\mathrm{B}}T$. For each trajectory consisting of 2^{19} time steps (step width $\Delta\bar{t}=0.001$) the power spectrum was calculated, and weighted and averaged according to Eq. (5). For the final spectrum typically 40 000 trajectories were recorded. Since these kinds of calculations are relatively cheap we chose a numerical accuracy of $1{:}10^{32}$.

Note that the trajectory calculations only consider collisions which start and end at large distances where forces practically vanish. As a consequence, bound states of particles in potential wells are not sampled by this method. As we have already shown in Paper I and is also confirmed below this effect is of no importance for the high-frequency spectra.

C. Evaluation of $g(r)$ at short distances

Our theory requires the knowledge of the potential of mean force. The corresponding radial distribution function $g(r)$ can in principle be derived from a classical molecular dynamics simulation. High-frequency spectra, however, are determined by rare high-energy collisions and, therefore, $g(r)$ has to be known at short distances which usually are not sampled properly by conventional molecular dynamics simulations. This problem is discussed extensively in Paper I. In order to evaluate the radial distribution function at short distances we applied a Monte Carlo (MC) method which relies on the following formalism.

The pair distribution function in a canonical ensemble of N particles is given by

$$g(r)=\mathrm{const}\,e^{-\beta V(r)}\int e^{-\beta V^{\mathrm{ex}}(\mathbf{r}_1,\ldots,\mathbf{r}_N)}d\mathbf{r}_3\cdots d\mathbf{r}_N, \tag{54}$$

where $r=|\mathbf{r}_1-\mathbf{r}_2|$ and

$$V^{\mathrm{ex}}(\mathbf{r}_1,\ldots,\mathbf{r}_N)=\sum_{2<i}V(\mathbf{r}_1-\mathbf{r}_i)+\sum_{2<j}V(\mathbf{r}_2-\mathbf{r}_j)+\sum_{2<i<j}V(\mathbf{r}_i-\mathbf{r}_j) \tag{55}$$

is the total potential energy with the exception of the direct potential between particles 1 and 2. In order to evaluate $g(r)$ at small distances, we define the cavity correlation function $y(r)$ by writing

$$g(r)=e^{-\beta V(r)}y(r). \tag{56}$$

While $g(r)$ strongly vanishes for small distances, the function $y(r)$ stays finite at the origin and can therefore be sampled much more easily by Monte Carlo methods.[35,36] Indeed, since

$$y(r)=\mathrm{const}\int e^{-\beta V^{\mathrm{ex}}(\mathbf{r}_1,\ldots,\mathbf{r}_N)}d\mathbf{r}_3\cdots d\mathbf{r}_N, \tag{57}$$

$y(r)$ can be interpreted as the radial distribution function of a fluid where all pairs of particles interact with potential $V(r)$, with the single exception of the pair 1 and 2. Because in this system particles 1 and 2 no longer repel each other, there are no sampling problems near $r=0$. To the contrary, in dense fluids the pressure from the other particles so often drives this pair to close distances, that it is difficult to sample the region of large distances which is needed to guarantee that $y(r)$ tends to 1 for large distances. In order to cope with this problem, we consider yet another system where all pairs of particles interact with potential $V(r)$ with the single exception of the pair 1 and 2 which interact with some mildly repulsive potential $\tilde{V}(r)$. We adjust $\tilde{V}(r)$ in such a way that the corresponding $\tilde{g}(r)$ can be sampled for the whole range of distances (umbrella sampling[37]). The precise form of $\tilde{V}$ is unimportant since $y(r)$ is independent of $\tilde{V}$. $y(r)$ is obtained from

$$y(r)=\tilde{g}(r)\,e^{\beta\tilde{V}(r)}. \tag{58}$$

In order to determine $\tilde{g}(r)$, MC calculations were performed with a canonical ensemble in a cubic simulation box with periodic boundary conditions. The thermodynamic conditions were similar to the MD simulations. For the interaction between particles 1 and 2 we chose a potential of the form

$$\tilde{V}(r)=A_0\exp\left[-4\left(\frac{r}{\sigma}\right)^2\ln 2\right], \tag{59}$$

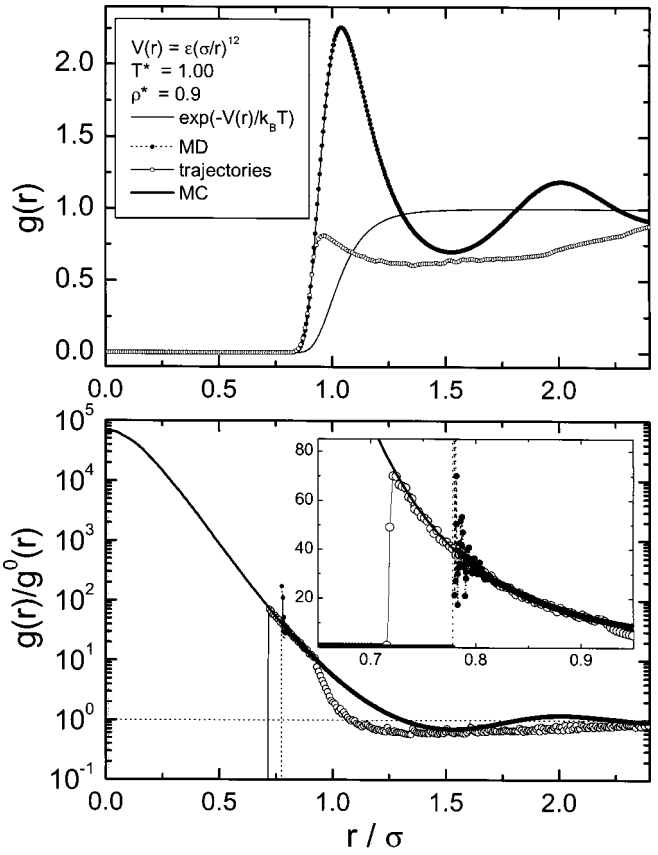

FIG. 1. Radial distribution functions for particles interacting via the repulsive potential $V_{12}(r)$ at $\bar{T}=1.0$ and $\bar{\rho}=0.9$. In the lower panel the cavity correlation functions are shown.

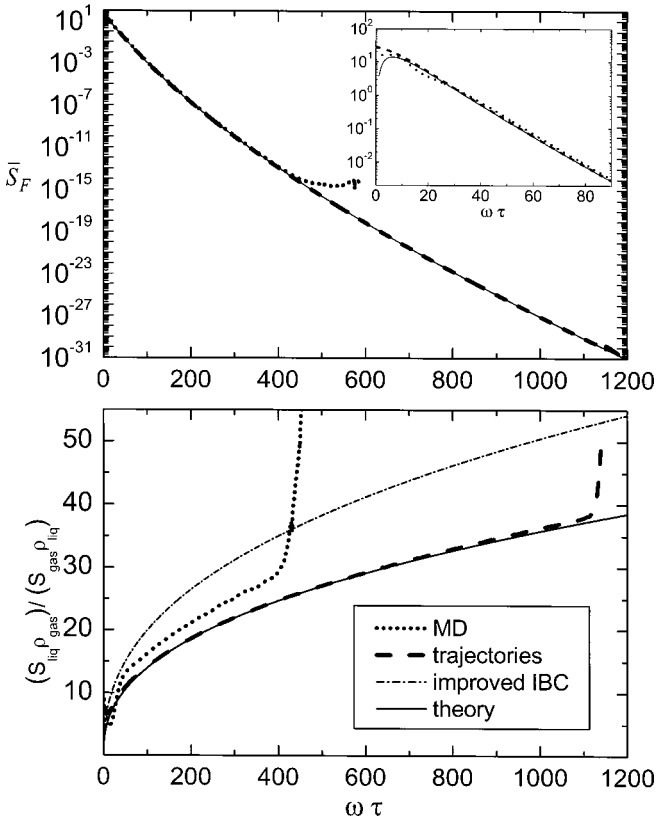

FIG. 2. Spectral densities of the breathing sphere force for the repulsive potential $V_{12}(r)$ at $\bar{T}=1.0$ and $\bar{\rho}=0.9$. The inset enlarges the low-frequency spectrum, whereas in the lower panel ratios of simulated to gas phase spectra are shown (see the text).

with $A_0 \sim 8k_BT$ and a σ which is the same as for the potentials of Eqs. (49) and (50) describing all the other pair interactions. After equilibration, up to 10^8 trials for each particle were taken to sample the configurational phase space. At every MC step the pair distribution between particle 1 and 2 was determined and averaged. This method yields $\tilde{g}(r)$ and by means of Eqs. (56) and (58) we obtain $g(r)$ apart from a constant factor. The scaling factor was obtained by comparing the MC result with the radial distribution function derived from the corresponding MD simulation at large distances were the latter method gives reliable results.

VI. COMPARISON BETWEEN THEORY AND COMPUTER SIMULATIONS

A. Repulsive potential V_{12}

Radial distribution functions play a key role in high-frequency spectra in liquids. In the upper panel of Fig. 1 the radial distribution function from a MD simulation of 500 particles interacting via the purely repulsive V_{12} potential at density $\bar{\rho}=0.9$ and temperature $\bar{T}=1.0$ is shown by black dots. For comparison, the low density limit $g^0(r)=\exp[-V(r)/k_BT]$ is also plotted by a thin line.

As expected, the MD result strongly deviates from the gas phase distribution due to the formation of a structured liquid. As is apparent from the lower panel of Fig. 1 where ratios $g(r)/g^0(r)$ are plotted, the MD curve ends at a certain distance $\bar{r}_{\min}=0.778$ which corresponds to the most energetic collision during the simulation. At shorter distances we obtained $g(r)$ by the Monte Carlo method described in the preceding section. The result is shown in the lower panel of Fig. 1 by a solid line. At large distances this curve is in complete agreement with the MD result. At short distances, however, it is well defined even for $\bar{r}\to 0$ where $y(r)=g(r)/g^0(r)$ reaches a maximum of $\sim 7\times 10^4$.

The MC radial distribution function is used to obtain the potential of mean force via $V_{\mathrm{mf}}(r)=-k_BT\ln g(r)$. As discussed previously, to calculate the spectra we approximate the liquid interacting with potential $V(r)$ by a hypothetical gas interacting with potential $V_{\mathrm{mf}}(r)$ (''mean field gas''). By definition, the liquid and the mean field gas then have the same radial distribution function. Since $V_{\mathrm{mf}}(r)$ is no longer purely repulsive, the trajectory calculations in the mean field gas do reproduce $g(r)$ only in the high-energy and small r region where the bound states become irrelevant. This is thoroughly discussed in Paper I. The open circles in Fig. 1 display the so determined radial distribution function in the mean field gas. Only in the very limited region $\bar{r}<0.92$, the calculations of $g(r)$ by trajectory and MC simulations do coincide. This, however, is the range relevant for the high-frequency spectra. For the trajectory simulations the maximum collision energy used was $50k_BT$. Via $V_{12}(\bar{r}_{\min})=E_{\max}$, this corresponds to $\bar{r}_{\min}=0.722$ in accord with Fig. 1.

Figure 2 displays the spectral densities $\bar{S}_F$ of the breath-

ing sphere force f_{12} of the repulsive potential V_{12}. The thick dotted curve is from the MD simulation, the thick dashed curve represents the trajectory result, and the thin solid line is the theoretical spectrum as derived from Eqs. (43) and (47). The frequency is given in units of τ^{-1} where τ is calculated from Eq. (14). For typical values of $\mu = 50\ \mathrm{g\,mol^{-1}}$, $\sigma = 0.4\ \mathrm{nm}$, and $\varepsilon/k_B = 100\ \mathrm{K}$, the value of $\omega\tau = 1$ corresponds to $\tilde{\nu} = \omega/2\pi c = 1.812\ \mathrm{cm^{-1}}$. The insert in the upper panel of Fig. 2 enlarges the low-frequency spectra, whereas in the lower panel ratios of the liquid phase spectra to the theoretical gas phase spectrum, normalized to the respective densities $(S_{\mathrm{liq}}\rho_{\mathrm{gas}})/(S_{\mathrm{gas}}\rho_{\mathrm{liq}})$ are plotted. This representation shows directly how the many-body effects change the spectrum when going from the gas to the liquid phase.

In principle, the MD calculation should give the most reliable spectrum. However, due to the limited numerical accuracy of 16 orders of magnitude, only the frequency range up to $\omega\tau \sim 400$ is accessible. But even below this, complications can occur due to finite simulation time (see Paper I). In order to demonstrate that the MD spectrum is actually accurate for $\omega\tau < 400$, return to the radial distribution function of Fig. 1. There we found agreement between MD and MC simulation down to $\overline{r}_{\mathrm{min}} = 0.778$. This corresponds to a maximum collision energy of $E_{\mathrm{max}} = 20.3\ k_B T$. According to Eq. (21) this energy corresponds to $\omega\tau \sim 570$ which is clearly above 400 and indicates that the MD spectrum is reliable in this region.

The trajectory spectrum covers 32 orders of magnitude since these calculations were performed with fourfold precision. As a result, the spectrum extends up to $\omega\tau \sim 1100$. A comparison between trajectory and MD result in $30 < \omega\tau < 400$ shows that the trajectory spectrum underestimates the true spectrum by about 10%. We attribute this difference to the mean field approximation, i.e., to the fact that fluctuations of the perturbing potential δV of the environment were neglected and only the potential of mean force was considered for the trajectory calculations. Nevertheless, the close agreement between both spectra indicates that the physical picture and theory developed in Sec. III are essentially correct.

The theoretical curve (thin solid line) is in perfect agreement with the trajectory calculation apart from the very low-frequency spectral region ($\omega\tau < 20$), where the theory is not applicable. This shows that within the mean field approximation the theory is asymptotically exact at high frequencies. In particular, the theory can be used to predict high-frequency spectral densities in regions which are not accessible by numerical methods.

Also shown in the lower panel of Fig. 2 is the improved IBC approximation of Eqs. (33) and (36) (dashed–dotted line). This spectrum overestimates the MD result by 20% and indicates that the main contribution of the environment to the spectra stems from the static quantity $g_{\mathrm{liq}}(r_0)/g_{\mathrm{gas}}(r_0)$. The force near the turning point is less important.

B. Lennard-Jones potential

In Fig. 3 radial distribution functions for the Lennard-Jones liquid at $\overline{T} = 1.0$ and $\overline{\rho} = 0.85$ are presented.

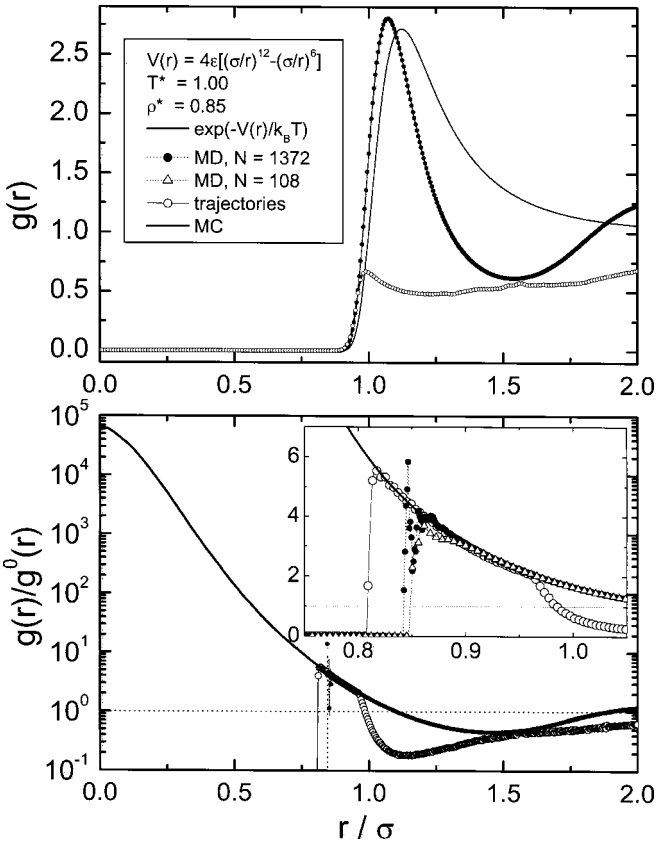

FIG. 3. Radial distribution functions for a Lennard-Jones liquid at $\overline{T} = 1.0$ and $\overline{\rho} = 0.85$. In the lower panel the cavity correlation functions are shown.

In the upper panel the MD result (black dots) was obtained from a simulation with 1372 particles. The low density limit $g^0(r)$ is shown for comparison. In the lower panel the ratio of both curves is plotted. The inset shows that the MD curve becomes noisy at short distances and ends at $\overline{r}_{\mathrm{min}} = 0.85$ corresponding to a maximum collision energy of $E_{\mathrm{max}} = 17.5 k_B T$ during the simulation. At shorter distances $g(r)$ can be explored only by the Monte Carlo method (full line). Also plotted in the inset is the result of a MD simulation with an ensemble of only 108 Lennard-Jones particles (open triangles). In this case the curve systematically goes below the MC result already at $\overline{r} < 0.89$ and ends at $\overline{r}_{\mathrm{min}} = 0.86$. In agreement with the analysis of finite particle numbers in the MD ensemble at gas phase conditions (see our previous paper[20]) we attribute the decrease of $g(r)/g^0(r)$ at $\overline{r} < 0.89$ to a finite-size effect. The consequences on the spectrum will be discussed below.

The radial distribution function defines the potential of mean force $V_{\mathrm{mf}}(r)$. As previously, we approximate the liquid spectra by the spectra of a hypothetical gas where the particles interact with this potential. Since bound states are omitted in the trajectory calculations, the $g(r)$ of the trajectory and MC calculations again coincide only for high energies or small distances, but this is all we need for the asymptotic spectra. The maximum collision energies for these trajectory simulations were $E_{\mathrm{max}} = 40 k_B T$. This corresponds to turning points at $\overline{r}_{\mathrm{min}} = 0.804$ in accord with Fig. 3.

In Fig. 4 we have plotted spectral densities $\overline{S_F}$ of the

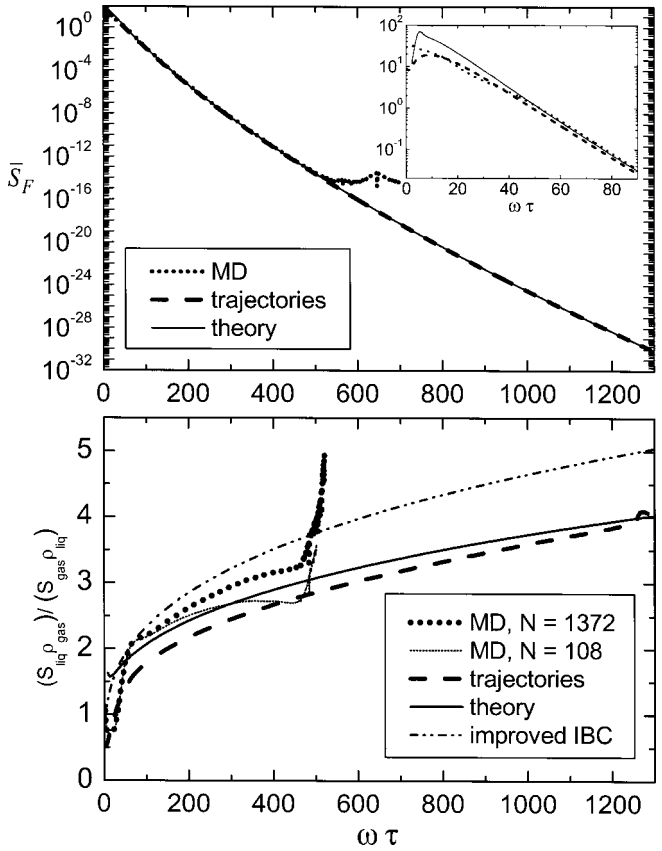

FIG. 4. Spectral densities of the breathing sphere force for a Lennard-Jones liquid at $\overline{T}=1.0$ and $\overline{\rho}=0.85$. The inset enlarges the low-frequency spectrum, whereas in the lower panel ratios of simulated to gas phase spectra are shown (see the text).

breathing sphere force for the Lennard-Jones liquid at $\overline{T}=1.0$ and $\overline{\rho}=0.85$. Bold dotted and dashed lines show the MD and trajectory results, respectively. The theoretical spectrum [Eqs. (43) and (45)] is the thin solid line. In the lower panel, where ratios of $(S_{\mathrm{liq}}\rho_{\mathrm{gas}})/(S_{\mathrm{gas}}\rho_{\mathrm{liq}})$ are plotted, we have included the MD results for 108 particles. Using Eq. (24) the cutoff of $g(r)$ at $\overline{r}_{\mathrm{min}}=0.85$ in Fig. 3 indicates that the spectrum is reliable up to $\omega\tau\sim 750$ which is well above the limit of $\omega\tau<450$ set by the numerical accuracy of the MD calculations. The MD spectral density obtained from the ensemble of 108 particles at $\omega\tau>200$ starts to fall below the spectrum with 1372 particles. This is in accord with the corresponding radial distribution function shown in Fig. 3 which at $\overline{r}<0.89$ is smaller than expected. Central collisions with turning points at $\overline{r}=0.89$ correspond to collision energies of $E=8.1k_{\mathrm{B}}T$. According to Eq. (24) these events contribute to the spectrum at $\omega\tau\sim 300$. At higher frequency the spectral density is smaller than for the larger ensemble since strong collisions are under-represented. As mentioned previously, this is probably a finite-size effect.

At high frequencies the spectrum from the trajectories underestimates the true spectrum by 15%. This indicates that the mean field approximation is appropriate to describe the influence of the liquid environment on binary collisions. The theoretical spectrum of Eq. (43) is about 10% below the true spectrum and slowly converges to the trajectory spectrum (thin solid line). Figure 4 shows that the improved IBC approach of Eqs. (33) and (36) also gives satisfactory results. The corresponding spectrum overestimates the MD calculation by about 10%.

VII. CONCLUSIONS

In this paper, we have applied a theory of high-frequency spectra in dense classical liquids to the phenomenon of vibrational energy relaxation employing the breathing sphere model. The theory is based on analytical expressions which represent exact asymptotic forms of spectra in classical gases at high frequency. In order to derive the corresponding spectra for the dense liquid, we note that high-frequency spectra are dominated by rare binary collisions, and that during these collisions the environment is practically frozen. In this way the environment influences the binary interaction by an perturbing potential. Assuming that the fluctuations of the environment are of minor importance, the perturbing potential is identified with the potential of mean force. The final expressions require knowledge of the radial distribution function at short distances. The latter is obtained by an importance sampling Monte Carlo calculation.

For the repulsive V_{12} and the Lennard-Jones potential the theoretical spectra are compared with conventional molecular dynamics and trajectory simulations of binary collisions in the relevant potential of mean force. The general agreement between all the spectra at high frequency is good. Deviation are of the order of 10–15 % indicating that the theory can be used to accurately predict spectral densities at regions which are not accessible by numerical methods. As in the gas phase, the spectra are of stretched exponential form which is in contrast to the popular exponential energy gap law. Our results are of general relevance and not limited to the breathing sphere model.

[1] J. Chesnoy and G. M. Gale, Ann. Phys. (Paris) **9**, 893 (1984).
[2] H. Hippler and J. Troe, in *Bimolecular Collisions*, edited by M. N. R. Ashfold and J. E. Baggott (The Royal Society of London, London, 1989), p. 209.
[3] R. G. Gilbert and S. C. Smith, *Theory of Unimolecular and Recombination Reactions* (Blackwell Scientific, Oxford, 1990).
[4] J. C. Owrutsky, D. Raftery, and R. M. Hochstrasser, Annu. Rev. Phys. Chem. **45**, 519 (1994).
[5] G. W. Flynn, C. S. Parmenter, and A. M. Wodtke, J. Phys. Chem. **100**, 12817 (1996).
[6] J. Chesnoy and G. M. Gale, Adv. Chem. Phys. **70**, 297 (1988).
[7] C. B. Harris, D. E. Smith, and D. J. Russell, Chem. Rev. **90**, 481 (1990).
[8] T. Elsaesser and W. Kaiser, Annu. Rev. Phys. Chem. **42**, 83 (1991).
[9] Y. Deng, B. M. Ladanyi, and R. M. Stratt, J. Chem. Phys. **117**, 10752 (2002).
[10] R. Zwanzig, J. Chem. Phys. **34**, 1931 (1961).
[11] R. M. Whitnell, K. R. Wilson, and J. T. Hynes, J. Phys. Chem. **94**, 8625 (1990).
[12] R. M. Whitnell, K. R. Wilson, and J. T. Hynes, J. Chem. Phys. **96**, 5354 (1992).
[13] M. Tuckerman and B. J. Berne, J. Chem. Phys. **98**, 7301 (1993).
[14] S. A. Adelman, R. Muralidhar, and R. H. Stote, J. Chem. Phys. **95**, 2738 (1991).
[15] D. W. Oxtoby, Adv. Chem. Phys. **47**, 487 (1981).
[16] J. S. Bader and B. J. Berne, J. Chem. Phys. **100**, 8359 (1994).
[17] K. F. Everitt and J. L. Skinner, J. Chem. Phys. **110**, 4467 (1999).
[18] K. F. Everitt, S. A. Egorov, and J. L. Skinner, Chem. Phys. **235**, 115 (1998).
[19] S. A. Egorov, K. F. Everitt, and J. L. Skinner, J. Phys. Chem. A **103**, 9494 (1999).

[20] D. Schwarzer and M. Teubner, J. Chem. Phys. **116**, 5680 (2002).
[21] A. Nitzan, S. Mukamel, and J. Jortner, J. Chem. Phys. **63**, 200 (1975).
[22] S. A. Egorov and J. L. Skinner, J. Chem. Phys. **105**, 7047 (1996).
[23] D. Rostkier-Edelstein, P. Graf, and A. Nitzan, J. Chem. Phys. **107**, 10470 (1997).
[24] L. D. Landau and E. A. Teller, Phys. Z. Sowjetunion **10**, 34 (1936).
[25] K. F. Herzfeld and T. A. Litovitz, *Absorption and Dispersion of Ultrasonic Waves* (Academic, New York, 1959).
[26] P. K. Davis and I. Oppenheim, J. Chem. Phys. **57**, 505 (1972).
[27] P. K. Davis, J. Chem. Phys. **57**, 517 (1972).
[28] C. Delalande and G. M. Gale, J. Chem. Phys. **71**, 4804 (1979).
[29] M. Teubner, Phys. Rev. E **65**, 031204 (2002).
[30] H. K. Shin, J. Chem. Phys. **56**, 2617 (1972). After the publication of the paper in Ref. 19 we discovered that Shin had studied the same problem. However, his paper contains a few errors that are mainly in the frequency-independent terms in our Eqs. (23) and (24). Using MATHEMATICA, we verified our results with Shin's method. In particular, in his Eq. (16) the denominator 144 should read 114 and the last term should read 19/114 D instead of 2/3 D. In his Eq. (17) the sign of the second to last term in the exponential must be negative. This changes the last term in the exponential of his Eq. (18) to $+0.5060$ D/kT from -0.838 D/kT.
[31] D. Forster, *Hydrodynamic Fluctuations, Broken Symmetries, and Correlation Functions* (W. A. Benjamin, Reading, MA, 1980).
[32] V. S. Vikhrenko, D. Schwarzer, and J. Schroeder, Phys. Chem. Chem. Phys. **3**, 1000 (2001).
[33] M. P. Allen and D. J. Tildesley, *Computer Simulation of Liquids* (Clarendon, Oxford, 1996).
[34] W. H. Press, S. A. Teukolsky, W. T. Vetterling, and B. P. Flannery, *Numerical Recipes in C* (Cambridge University Press, Cambridge, 1992).
[35] M. Llano-Restrepo and W. G. Chapman, J. Chem. Phys. **97**, 2046 (1992).
[36] M. Llano-Restrepo and W. G. Chapman, J. Chem. Phys. **100**, 5139 (1994).
[37] G. Torrie and G. N. Patey, Mol. Phys. **34**, 1623 (1977).